Optimal trajectories for soft landing on asteroids

Space Systems Design Lab
Georgia Tech Aerospace Eng.

AE8900 MS Special Problems Report
Space Systems Design Lab (SSDL)
School of Aerospace Engineering
Georgia Institute of Technology
Atlanta, GA

Author
Gregory Lantoine

Advisor
Dr. Robert Braun
Space Systems Design Lab (SSDL)

December 15, 2006

Optimal trajectories for soft landing on asteroids

G. Lantoine* and R. D. Braun+

Georgia Institute of Technology
Guggenheim School of Aerospace Engineering

Robotic exploration of asteroids has been identified by NASA as a major long-term goal. Central to many asteroid missions is a precise soft landing to enable surface exploration or exploitation. This paper describes a technique for computing optimal autonomous controlled trajectories for soft landing in an irregular gravity field of a rotating asteroid. We will first discuss the complexity of the forces that act on the spacecraft during a landing and how we can model them. Then, we will present the numerical method used to solve the optimal control problem, and typical results are shown on case studies at asteroids Vesta and Golevka. In each example, we will identify the best mission design scenarios, as well as some operational difficulties. Finally, we will investigate sensitivity to parameter uncertainties and the implementation of a real-time feedback controller to increase landing accuracy.

Nomenclature

G = gravitational constant
μ = gravitational parameter
U = gravitational potential
ρ = density
w = rotation rate
V_{ex} = exhaust gas velocity
m = mass of the spacecraft

I Introduction

NASA's Solar System Exploration Roadmap,[1] unveiled in 2004, outlines the major goals of the United States Solar System exploration program for the coming decades. Among the most prominent goals is NASA's mission to "explore […] asteroids, and other bodies to search for evidence of life, to understand the history of the solar system, and to search for resources." In response to this interest, NASA and the other world's space agencies have been planning and performing missions to small celestial objects.

To explore effectively asteroids, landing is necessary since this allows to perform in situ measurements or to exploit resources. However, this is a challenging step due to the remoteness of these bodies, their wide range of shapes and their complex gravitational fields.

To date, only two descents to an asteroid surface were successfully implemented : one by NASA's Near Earth Asteroid Rendezvous (NEAR) spacecraft on Eros using a series of open-loop thrusts,[2] the other by the Japan Aerospace Exploration Agency's Hayabusa sample return mission on Itokawa.

This study addresses some of the basic questions that must be dealt with in that situation, with an emphasis on parking orbit and trajectory design. An original combination of two direct and indirect techniques is used in this paper to find minimum time and minimum fuel optimal trajectories.

Since extremely irregular and diverse asteroid shapes can be encountered, we need to pay special attention to their shape modeling. We chose to approximate a body by a homogeneous polyhedron with a variable number of triangular faces. This shape model can be obtained from terrestrial observations (photometric or radar data), as well as from spacecraft observations, and gives the radius of the asteroid at multiple locations. Also this approximation can be very accurate since very complex geometries (cliffs, holes...) can be simulated.

After modeling the dynamical environment and presenting the way to solve the problem, we will study two practical examples with asteroids Vesta and Golevka. They are dramatically different and embrace a wide range of physical parameters. Fig. 1 shows their polyhedral shape models from data found on the NASA asteroid database website.[3] Important parameters of these two asteroids are listed in Table 1.

* Teaching Assistant, School of Aerospace Engineering, 270 Ferst Dr., AIAA Student Member
+ Associate Professor, School of Aerospace Engineering, 270 Ferst Dr., AIAA Associate Fellow.

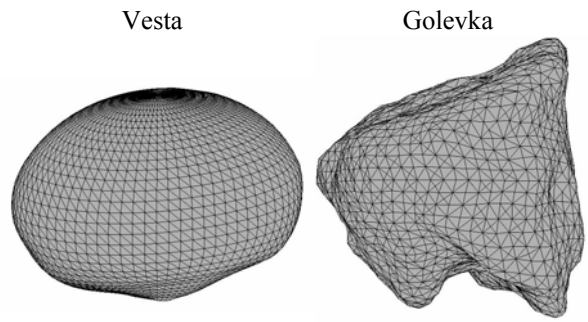

Fig. 1 Shapes of Vesta and Golevka

	Vesta	Golevka
Category	Main Belt	Mars-crosser
Mean diameter	530 km	0.53 km
Mass	$2.70\ 10^{20}$ kg	$2.10\ 10^{11}$ kg
Density	3.4 g/cm^3	2.7 g/cm^3
Rotation period	5.34 h	6.03 h

Table 1 Physical parameters of Vesta and Golevka

While Vesta's shape is very close to a perfect triaxial ellipsoid, Golevka has a very strange and angular shape that will induce a very irregular gravity field. The magnitude of its gravity field will be also extremely low since it is a very small object (Vesta is one thousand times bigger).

II Dynamical environment modeling

In the vicinity of an asteroid, a spacecraft is subject to :

- the central asteroid gravitational attraction
- the solar radiation pressure

The sun gravitational force is not taken into account because it is not expected to have a significant effect close to the asteroid.

II.A Gravitational attraction

There are several approaches to model the gravitational attraction of a non-spherical body, each of them with advantages and drawbacks.

II.A.1 Polyhedron potential

The exterior gravitational potential of a constant-density polyhedron was derived analytically by Werner and Scheeres.[4]

$$U = \frac{1}{2} G\rho \sum_{e \in edges} \mathbf{r_e}.\mathbf{E_e}.\mathbf{r_e}.L_e - \frac{1}{2} G\rho \sum_{f \in faces} \mathbf{r_f}.\mathbf{E_f}.\mathbf{r_f}.w_f$$

where $\mathbf{r_e}$ is a vector from the field point to an arbitrary point on each edge, $\mathbf{E_e}$ is a dyad defined in terms of the face and edge normal vectors associated with each edge, L_e is a logarithmic term expressing the potential of a 1D straight wire, $\mathbf{r_f}$ is a vector from the field point to an arbitrary point on each face, $\mathbf{F_f}$ is the outer product of face normal vectors, w_f is the solid angle subtended by a face when viewed from the field point.

The main advantage of this method is that it gives the exact potential of the polyhedron anywhere in space. The only possible sources of errors are then the adequacy of the polyhedral shape modeling and local variations in density.

However, this formula involves the computation of sums over all the edges and all the faces of the polyhedron. Since an accurate shape model requires a large number of faces and edges, this approach is computational intensive, particularly when implemented in Matlab since it is very slow to execute loops. A way to limit this issue is to code this algorithm by running Mex-functions in Matlab written in C. To evaluate the efficiency of this method, we compared the computational time needed to integrate the body-fixed equations of motion over one period for a spacecraft in orbit around a sphere modeled by a 16,471-vertices polyhedron. The equations of motion are integrated using Matlab's "ode45" function (Dormand–Prince method) with a relative tolerance of 10^{-6} (m) and an absolute tolerance of 10^{-8} (m).

m-function	Mex-function
13 h	1 min

Table 2 Comparison of computation times

We can see that the implementation using a Mex-function leads to a huge reduction in computation time (around one thousand times faster). However, as we will see later in the paper, highly nonlinear optimization problems require a very long optimization time with thousands of iterations, so this is still a significant time, and we may need a faster approach.

II.A.2 Spherical Harmonic Expansion

The exterior gravitational potential of any object can be classically expressed as an infinite series expansion in solid spherical harmonics.

$$U = \frac{GM}{r}\left\{1 + \sum_{n=1}^{\infty}\left(\frac{R_e}{r}\right)^n \sum_{m=0}^{n} P_{n,m}(\sin\lambda) \left[C_{n,m}\cos(m\phi) + S_{n,m}\sin(m\phi)\right]\right\}$$

where M is the total mass of the body , R_e is its largest equatorial radius, (r,λ,ϕ) are the radius, latitude and longitude of the field point, $P_{n,m}$ are the associated Legendre functions, $C_{n,m}$ and $S_{n,m}$ are the harmonic

coefficients. They represent the mass distribution of the body. They are computed using a polyhedral shape and the recurrent relationships derived by Werner.[5]

Finite truncations are often sufficient to get good accuracy, therefore this approach is easy and fast to use. The drawback is that severe divergence appears close to the body's surface. Thus this model is not recommended to compute the asteroid's gravity at close range. An example of this phenomenon applied at Golevka is displayed below.

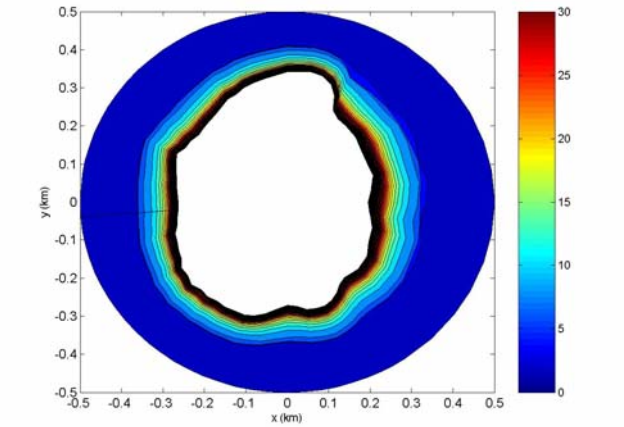

Fig. 2 Error (%) of the spherical harmonic potential relative to the polyhedral potential for Golevka (xy plane)

As shown in Fig. 2, the spherical harmonic model begins to diverge at the 0.4 km radial distance. Since the polyhedron gravity model is computationally more intensive, we need to find a compromise between speed and accuracy. One way is to perform a transition from the spherical harmonic model to the polyhedron model when the spacecraft's radial distance moves inside 0.4 km. We applied a similar strategy at Vesta.

II.B Solar radiation pressure

We assume that the solar radiation pressure varies according to an inverse-square law with the distance from the sun and acts along the line joining the sun and the small body.

$$\mathbf{F_S} = \frac{G}{BR^2}\mathbf{r_g}$$

where $\mathbf{r_g}$ is the unit vector from the sun to the small body, R is the sun-small body distance, and B is the spacecraft mass to projected area ratio. We supposed in the following a value of 40 kg/m^2 for B (approximate value for the NEAR spacecraft).[6]

However, this force has a significant contribution only for very small asteroids with low gravity field, therefore we will neglect it in the study of Vesta.

II.C Validation of the model

Before solving the landing problem, we needed to ensure that our code worked as intended. Since the data of NEAR landing trajectory are published,[2] this was a good opportunity to use it as a test case and compare the simulation output to the real trajectory. The spacecraft transitioned from an orbit about Eros into a ballistic trajectory and four maneuvers were used to deorbit and control the impact speed. Therefore, we propagated our work from the same initial conditions as the NEAR mission including maneuvers at the same time as NEAR. Fig. 3 gives the altitude profile for the NEAR mission and our computed trajectory. The results show very good agreement.

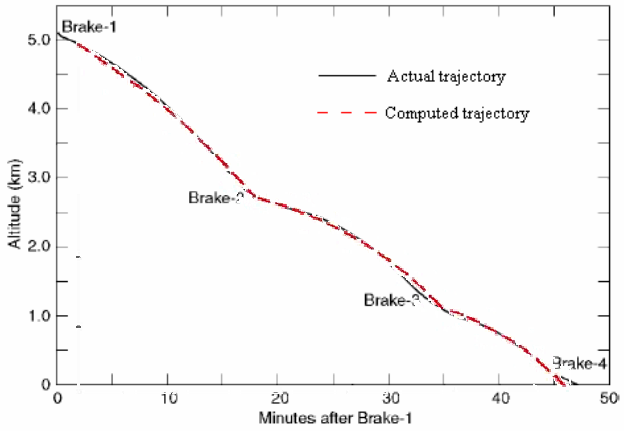

Fig. 3 Comparison of descent profiles

III Problem formulation

III.A Governing equations

The equations of motion are expressed in the small-body-fixed Cartesian coordinate frame with origin at the body's center of mass. The trajectory is controlled by the spacecraft's thrusters.

$$\begin{cases} \ddot{x} = 2w\dot{y} + w^2 x - \dfrac{\partial U}{\partial x} + F_{Sx}(t) + \dfrac{T}{m}\cos\beta\cos\theta \\ \ddot{y} = -2w\dot{x} + w^2 y - \dfrac{\partial U}{\partial y} + F_{Sy}(t) + \dfrac{T}{m}\cos\beta\sin\theta \\ \ddot{z} = -\dfrac{\partial U}{\partial z} + F_{Sz}(t) + \dfrac{T}{m}\sin\beta \\ \dot{m} = -\dfrac{T}{V_{ex}} \end{cases} \quad (1)$$

where T is the thrust magnitude ($0 \le T \le T_{max}$), β and θ are the latitude and longitude angle directions respectively.

Consider the state vector **x** = [*x, y, z, Vx, Vy, Vz, m*] and the control vector **u** = [T, β, *θ*]. The equations motions can then be summarized by a single formula :

$$\dot{\mathbf{x}} = \mathbf{f}(\mathbf{x}, \mathbf{u}, t)$$

III.B Boundary conditions

The spacecraft can start from a parking orbit or a specified location. Its initial mass is known. These conditions can be expressed at the initial time by :

$$\begin{cases} \psi(x, y, z, V_x, V_y, V_z)\big|_0 = 0 \\ m(0) = m_0 \end{cases} \quad (2)$$

Regarding the final conditions, the coordinates of the landing site are fixed and the vehicle must land with zero velocity at the surface. The final mass is kept free but must stay above a minimum value (dry mass) :

$$\begin{aligned} & x(t_f) = x_f, y(t_f) = y_f, z(t_f) = z_f, \\ & V_x(t_f) = 0, V_y(t_f) = 0, V_z(t_f) = 0, \\ & m(t_f) \geq m_{dry} \end{aligned} \quad (3)$$

III.C Formulation of the optimization problem

An optimization problem is any problem where it is desired to minimize a specified criterion, referred to as a cost function. In this study, we will use two criteria :

- descent duration : during landing, the spacecraft is subject to perturbing forces (solar gravitational force, dust…). These forces and other parameter uncertainties will influence the motion of the lander. Therefore, the shorter the duration is, the greater the landing robustness with respect to model uncertainties.
- fuel consumption to minimize the mass of propellant and therefore the cost of the mission.

We will compare the optimal trajectories obtained with either criterion.

In our study, the cost function is of the form

$$J(\mathbf{u}) = \phi(\mathbf{x}(t_f), t_f)$$

where $\phi = t$ for optimal time strategy or $\phi = -m$ for optimal fuel strategy. The problem is to find a control function **u*** that minimizes *J*, subjected to the governing equations (1) and the boundary conditions (2) and (3) described in the previous sections.

In summary, we have to deal with a complex nonlinear two-point boundary optimization problem. An approach for the solution is discussed in detail in the following sections. First, we present the optimal control theory that gives all the necessary information to find an exact solution.

III.D Optimization theory

The Pontryagin Principle is employed.[7] According to this theory, the optimal control **u*** is obtained by minimizing the Hamiltonian *H* with respect to **u** :

$$\mathbf{u}^* = \arg\min_u H$$

where *H* is expressed by :

$$H = \lambda_x V_x + \lambda_y V_y + \lambda_z V_z + \lambda_{Vx}\dot{V}_x + \lambda_{Vy}\dot{V}_y + \lambda_{Vz}\dot{V}_z + \lambda_m \dot{m}$$

and $\lambda_x, \lambda_y, \lambda_z, \lambda_{Vx}, \lambda_{Vy}, \lambda_{Vz}, \lambda_m$ are the components of the adjoint vector satisfying the differential equations (which are not given in detail here) :

$$\dot{\boldsymbol{\lambda}}^T = -\frac{\partial H}{\partial \mathbf{x}} \quad (4)$$

Substituting the equations of motion into the expression of *H*, it follows that

$$H = g(\mathbf{x}, \boldsymbol{\lambda}) + \underbrace{\left(\frac{\lambda_{Vx}}{m}\cos\beta\cos\theta + \frac{\lambda_{Vx}}{m}\cos\beta\sin\theta + \frac{\lambda_{Vz}}{m}\sin\beta - \frac{\lambda_m}{V_{ex}}\right)T}_{S(t)}$$

where *g* is a function of **x** and *λ* only, and *S* is the so-called switching function (coefficient of *T* in the Hamiltonian).

Applying the Pontryagin Principle, we obtain the following expressions of the optimal controls :

- optimal θ :

$$\frac{\partial H}{\partial \theta} = 0 \quad \rightarrow \theta^* = \operatorname{atan}\left(\frac{\lambda_{Vy}}{\lambda_{Vz}}\right) \quad (5)$$

By this condition only, θ is not uniquely defined since $0 \leq \theta \leq 2\pi$. The quadrant of θ in the trigonometric circle is found by using the following second order condition :

$\frac{\partial^2 H}{\partial \theta^2} > 0$. After calculations, we get sign θ = -sign λ_{Vy}.

- optimal β :

$$\frac{\partial H}{\partial \beta} = 0 \quad \rightarrow \beta^* = \operatorname{atan}\left(\frac{\lambda_{Vz}}{\lambda_{Vx}\cos\theta^* + \lambda_{Vy}\sin\theta^*}\right) \quad (6)$$

In that case, β is uniquely defined since $-\pi/2 \leq \beta \leq \pi/2$.

- optimal *T* :

The situation is different than the two previous cases since *H* is linear in *T*, which is bounded. Application of Pontryagin Principle leads to pushing *T* to its upper or lower bound depending on the sign of the switching function in the Hamiltonian. This is referred as a bang bang solution.

$$H = g + ST \quad \rightarrow T^* = \begin{cases} 0 & \text{if } S > 0 \\ T_{\max} & \text{if } S < 0 \end{cases} \quad (7)$$

III.E Method of solution

Numerical methods to solve optimal control problems fall into two distinct categories: direct and indirect. An indirect method uses information from the co-state differential equations, the Pontryagin principle, and the boundary conditions, to find the optimal solution. This is accurate and fast, but the domain of convergence is very low, i.e. convergency depends highly on the accuracy of an initial estimate. In addition, an estimate of the co-states is required a priori, which is difficult to figure out since they do not have physical significance. An easier approach is to use a direct method, which aims at directly optimizing the cost function. It is characterized by a robust convergency even against a poor initial estimate – and no estimates of co-states are required –, but computation time significantly increases with number of time steps to obtain more accuracy.

From these characteristics, we chose to combine the two methods to solve the problem in a practical basis. First, we integrate the equations of motion backwards in time from the known landing site and using a 'common sense' control law to obtain a rough estimate. Then we run the direct code with a small number of time steps. Finally, we use the result to run the indirect code with a large number of time steps to get a final estimate.

III.F Implementation

The Matlab software package DIDO[8] is used to implement the direct method. It is easy to use and is capable of solving a wide variety of problems. More precisely, it employs the Legendre Pseudospectral Method which fits globally orthogonal polynomials to the discrete data over the entire time span.

The Fortran routine BNDSCO[9] is used to implement the indirect method. It is a multiple shooting method. Central to a shooting method is the ability to integrate the differential equations as an initial value problem with guesses for the unknown initial values.

Typical computation time for solving the landing problem is plotted in Fig. 4 as a function of number of nodes. All calculations were conducted on a Pentium 4 PC computer (1.9 MHz). In the combined method, initial estimates were calculated using the DIDO code with 100 time steps (minimum required for the indirect method to converge) and final estimates were obtained by the BNDSCO code. We can see in Fig. 4 that the computation time for the direct method significantly increases with number of time steps while it only slightly increases in the combined method. Therefore, our approach leads to huge save of computation time without spoiling accuracy and convergence.

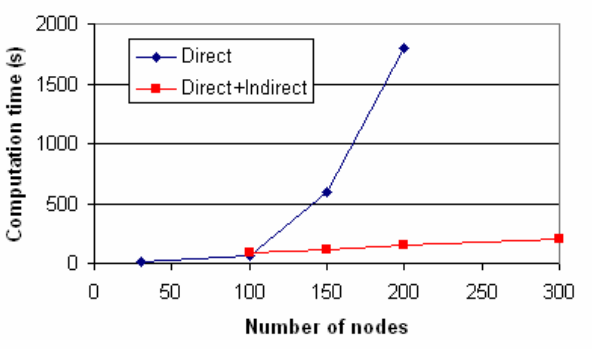

Fig. 4 Typical computation time for the landing problem

IV Landing simulation on Vesta

IV.A Assumptions

Spacecraft characteristics similar to NEAR were chosen, which corresponds to an engine's maximum thrust limit of 650 N and a specific impulse of 330 s. The vehicle has a dry mass of 487 kg and we assume that it carries onboard 75 kg of propellant before landing. The solar panels are fixed relative to the spacecraft's body.

The spacecraft starts from a nearly circular parking orbit. However, since Vesta is not spherical, the existence of such orbit is not trivial and this is the object of the following section.

IV.B Design of the parking orbit

IV.B.1 Orbit stability analysis

The question of orbit stability around Vesta has to be addressed. In fact, if it is unstable, the spacecraft might collide with Vesta or escape from orbit.

Large energy variation over one orbit period often traduces instability. Therefore, we estimate the maximum change in energy over one orbit of semi-major axis a and inclination i :[10]

$$\left\|\frac{\Delta E}{E}\right\| \le \frac{12\overline{C}_{22}}{\sigma^{4/3}(\sigma^2-1)}\left|\sin(2\pi\sigma)\right|\left[\cos i + \frac{1}{2}\sigma(1+\cos^2 i)\right]$$

where

$\overline{C}_{22} = C_{22}(R_e / r_S)^2, r_S = (\mu / w^2)^{1/3}, \sigma = a^{3/2} w / \sqrt{\mu}$

and $r_S \approx 550$ km is the so-called resonance radius at which centripetal acceleration is equal and opposite to gravitational acceleration.

This function is plotted in Fig. 5. It was found that the transition from stability to instability corresponds approximately to a 5% fluctuation in energy over one orbit.[10]

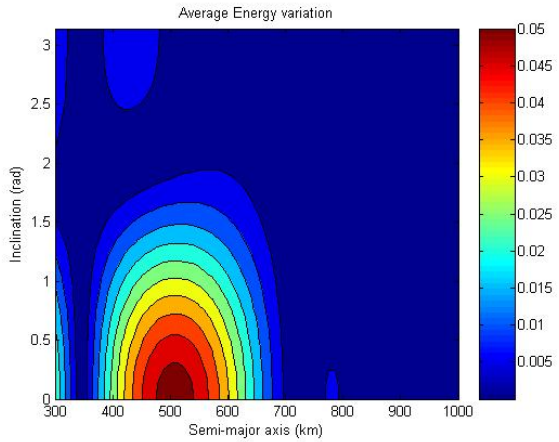

Fig. 5 Average Energy variation

We can see that direct orbits between 400 and 600 km – those close to the resonance radius – are likely to be unstable. In fact, instabilities are generally closely related to resonances between the central body's rotation rate and the mean motion of the spacecraft.

To have a stable orbit relatively close to the surface at any inclination, we selected a semi-major axis of 350 km for our parking orbit.

IV.B.2 Determination of circular periodic orbits

In addition for being stable, the parking orbit needs to be preferably circular periodic – or at least nearly circular periodic – to predict easily the position of the spacecraft and have a simple function to describe the orbit.

Since Vesta is not spherical, we cannot avoid a variation in the ascending node for any orbit due to the effect of zonal harmonics. Therefore, nearly circular periodic orbits can exist only in a reference frame regressing about the Z axis at the nodal regression rate (supposed constant). Following Wiesel[11], we developed an algorithm to find these orbits for any inclination and orbital radius. First we take initial conditions on the X axis with a fixed initial inclination i and fixed initial radius r_0 :

$$x = r_0\,, \quad y = 0\,, \quad z = 0,$$
$$V_x = \dot{r}_0\,, \quad V_y = Vt_0 \cos i\,, \quad V_z = Vt_0 \sin i$$

The unknown parameters are the period τ , the radial velocity $\dot{r}_0$, and the tangential speed Vt_0. To find them, we state that the satellite must again be crossing the plane Z=0, be at the same distance from Vesta r_0, and have the same flight path angle after one period, which corresponds to the following final conditions :

$$z(\tau) = 0\,, \quad r(\tau) = r_0\,, \quad \mathbf{r}(\tau).\mathbf{V}(\tau) = r_0\,\dot{r}_0$$

This is a simple two-point boundary problem and was basically solved with the function *fsolve* in Matlab using the keplerian values as a first guess.

A solution for r = 350 km and i = 80° is plotted after 10 periods in Fig. 6. Its actual period is 187 min while the corresponding keplerian value is 189 min, which corresponds to a difference of 1 %.

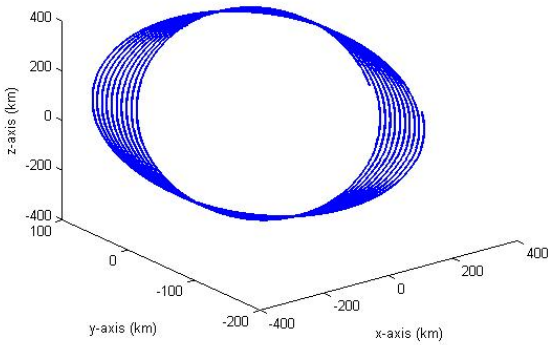

Fig. 6 Orbit in inertial frame

We can check if this orbit is really periodic in the 'nodal-fixed frame'. For that, we calculate the amount of rotation about the Z axis between the initial position and the position after one period :

$$\cos\theta = \mathbf{r}(0).\mathbf{r}(\tau) / r_0^2$$

Then the regression rate of the ascending node is

$$\dot{\Omega} = -\theta / \tau$$

and the corresponding rotation matrix is

$$\Re = \begin{pmatrix} \cos(\Omega_0 + \dot{\Omega}t) & \sin(\Omega_0 + \dot{\Omega}t) & 0 \\ -\sin(\Omega_0 + \dot{\Omega}t) & \cos(\Omega_0 + \dot{\Omega}t) & 0 \\ 0 & 0 & 1 \end{pmatrix}$$

Using this rotation matrix, the trajectory in the nodal-fixed frame is plotted in Fig. 7. After 10 periods, it still has a circular periodic shape, which proves the efficiency of the algorithm.

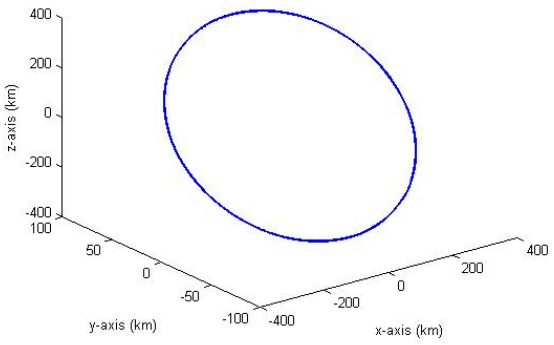

Fig. 7 Orbit in nodal-fixed frame

Our strategy will then to use first keplerian values and run DIDO to find the optimal inclination. Then we use this algorithm to find the corresponding near circular periodic orbit and the corresponding velocity. Finally we run DIDO again with this new initial condition.

IV.B.3 Mission constraints

The most important mission constraint to satisfy relates to solar panel illumination. In general, the normal of the solar arrays must remain within 30° of the Sun direction to generate enough power. For any scientific mission, it is of course necessary to point the instruments and hence the spacecraft at the asteroid we want to study. Therefore, since we supposed that the solar panels are fixed relative to the spacecraft, the orbit plane must stay within 30° of the Sun Plane-Of-Sky (SPOS) whose normal is along the sun-asteroid line direction. Then from the inclination of the SPOS relative to the Z axis, we can deduce the range of allowed inclinations of the parking orbit.

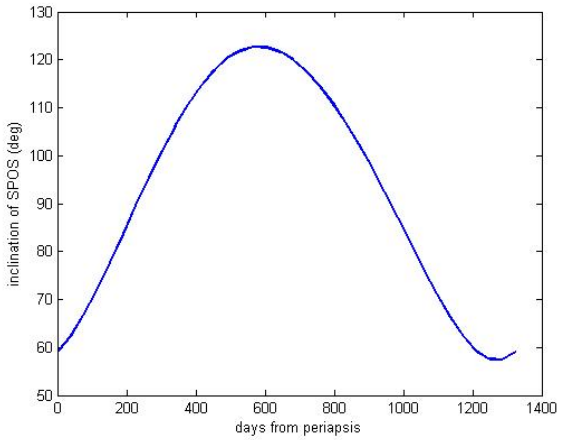

Fig. 8 SPOS inclination over one period of Vesta

The mission is likely to take place when Vesta crosses the ecliptic plane. At that location, the inclination of SPOS is 86°. It follows that the inclination of the parking orbit must satisfy $56° \le i \le 124°$.

IV.C Two-Point Boundary Value Problem formulation

IV.C.1 Initial conditions

The initial conditions must satisfy the following relations since powered braking starts from any position of a circular orbit :

$$\begin{cases} x_0^{\,2} + y_0^{\,2} + z_0^{\,2} = r^2 \\ Vx_0^{\,2} + Vy_0^{\,2} + Vz_0^{\,2} = V^2 \quad \Rightarrow \psi(\mathbf{x},0) = 0 \\ x_0 Vx_0 + y_0 Vy_0 + z_0 Vz_0 = 0 \end{cases} \tag{8}$$

These relations give information about the initial values of the state variables at the initial time t_i. However the initial values for the co-state variables are still unknown and hence we need additional equations. For that, we introduce new parameters ν and we classically define the auxiliary function Φ as the following :

$$\Phi = \phi + \nu^T \psi$$

Then, from the optimal control theory,[7] we can find that

$$\lambda^T(0) = \Phi_x\big|_{t=0}$$

Eliminating ν, we get the three extra relations involving the co-states we were looking for :

$$\begin{aligned}&(z_0 Vx_0 - x_0 Vz_0)(Vx_0 \lambda_{Vy}(0) - Vy_0 \lambda_{Vx}(0)) \\ &\quad -(y_0 Vx_0 - x_0 Vy_0)(Vx_0 \lambda_{Vz}(0) - Vz_0 \lambda_{Vx}(0)) = 0\end{aligned} \tag{9}$$

$$\begin{aligned}&(z_0 Vx_0 - x_0 Vz_0)(x_0 \lambda_z(0) - z_0 \lambda_x(0)) \\ &\quad -(x_0 Vz_0 - z_0 Vx_0)(Vx_0 \lambda_{Vz}(0) - Vz_0 \lambda_{Vx}(0)) = 0\end{aligned} \tag{10}$$

$$\begin{aligned}&(z_0 Vx_0 - x_0 Vz_0)(x_0 \lambda_y(0) - y_0 \lambda_x(0)) \\ &\quad -(x_0 Vy_0 - y_0 Vx_0)(Vx_0 \lambda_{Vz}(0) - Vz_0 \lambda_{Vx}(0)) = 0\end{aligned} \tag{11}$$

IV.C.2 Final conditions

The terminal conditions on the state variables are all specified by eq. (3) except on the mass. The Pontryagin Principle requires that the terminal value of a co-state variable corresponding to a free-state variable is to be equal to the derivative of the cost function relative to the corresponding state at the final instant of time. It follows that :

$$\lambda_m(t_f) = 0 \quad \text{in case of optimal time}$$

$$\lambda_m(t_f) = -1 \quad \text{in case of optimal fuel} \tag{12}$$

The other co-state variables are free at the final time since the terminal conditions of corresponding state variables are fixed by eq. (3).

Since the final time t_f is not known, the transversality condition yields and states that the Hamiltonian must be equal to the opposite of the derivative of the cost function relative to time :

$$H(t_f) = -1 \quad \text{in case of optimal time}$$

$$H(t_f) = 0 \quad \text{in case of optimal fuel} \tag{13}$$

IV.C.3 Summary

The landing problem on Vesta is converted into a two-point boundary value problem and is stated as follows : the differential equations (1) and (4) are to be solved with the boundary conditions (3) and (8)-(13), while the optimal controls are described by equations (5)-(7).

IV.D Simulation results

IV.D.1 Optimal time strategy

Details of the trajectory, including altitude, velocity, flight path angle, etc, are plotted in Figures 9 to 14. The direct solution is displayed with a dashed line and the indirect one with a solid line.

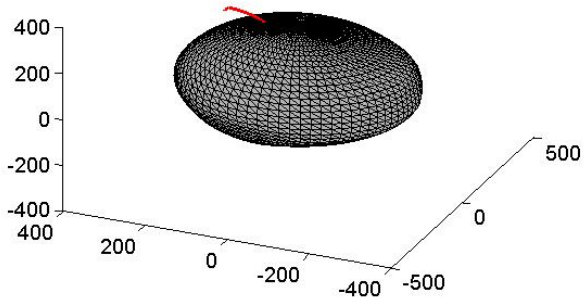

Fig. 9 Optimal-time trajectory

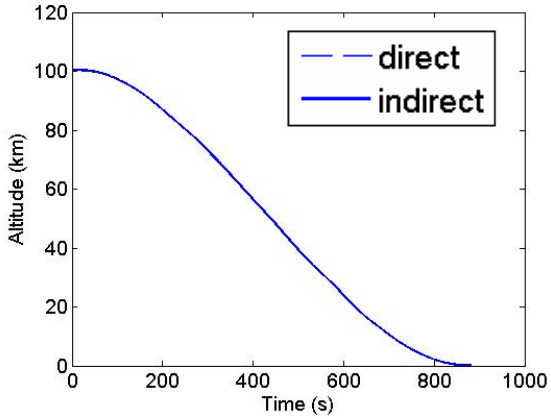

Fig. 10 Altitude

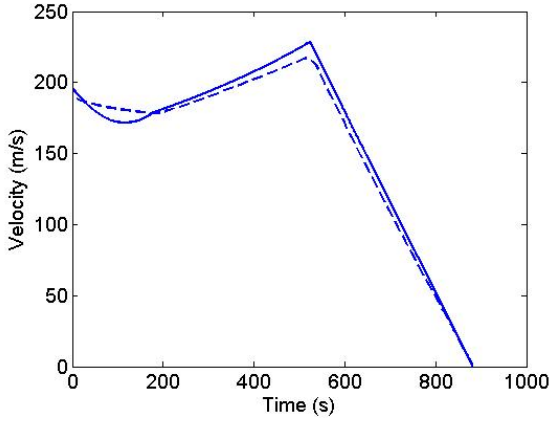

Fig. 11 Velocity magnitude

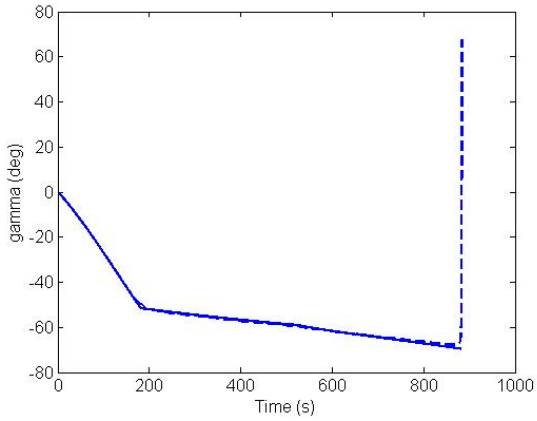

Fig. 12 Flight-Path angle

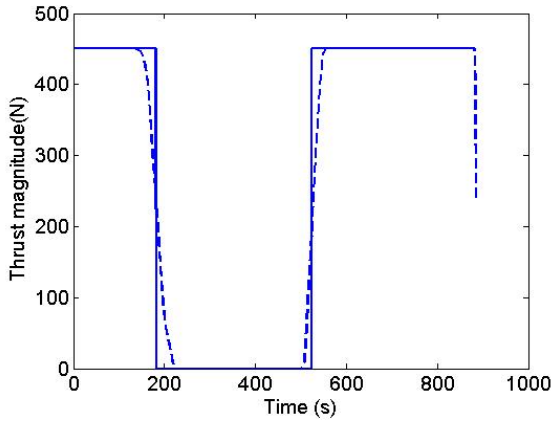

Fig. 13 Thrust magnitude

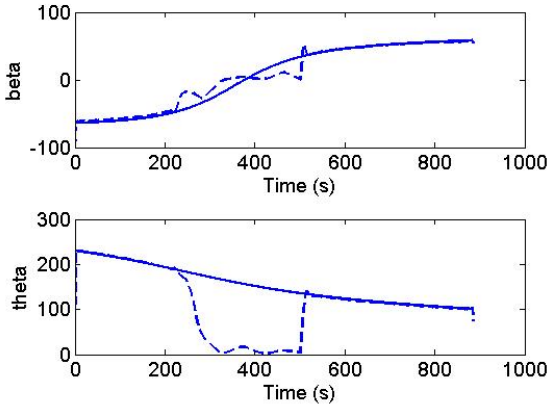

Fig. 14 Thrust directions

The thrust magnitude has an expected bang bang profile. The initial de-orbit burn has a duration of 185 s, followed by a descent coast of 354 s, and a final braking burn of 369 s.

When the engine is off, the thrust direction angles do not play any role, which explains the large difference during the descent coast between direct and indirect methods for these parameters.

The flight path angle starts at zero as the spacecraft is in a circular orbit about the Moon. It is seen to decrease linearly with slope discontinuities at thrust switches. The final relevant value of the flight path angle is approximately -70 deg, which suggests that the trajectory is largely vertical at landing, which is recommended from an operational standpoint.

The optimality of this solution is investigated next. Since the Hamiltonian is not a function of time, it should be constant and equal to zero. The Hamiltonians of both methods are displayed in Fig. 15. The DIDO estimate is fairly flat and is small in magnitude, but it is not constant. In particular, large peaks are seen at the end points of the time span, and small fluctuations are seen at the locations of the control discontinuities. It confirms that the direct solution is not optimal.

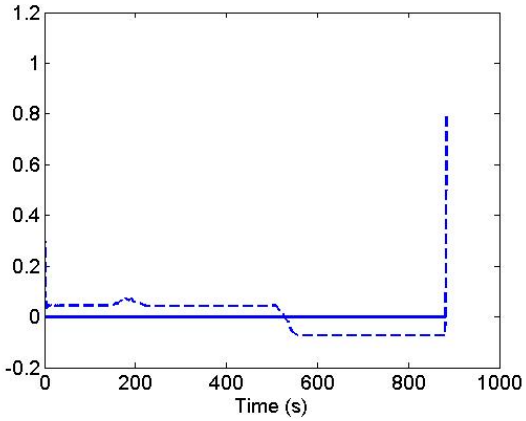

Fig. 15 Hamiltonian

The entire 75 kg of fuel available is consumed. That explains the presence of the descent coast since there was not enough propellant to have a constant-thrust solution. In fact, if we increase the initial mass of propellant and run the simulation again, we observe that the descent coast phase is reduced until a critical value of the initial fuel mass of around 100 kg corresponding to a constant-thrust solution. Therefore, the shape of the solution can be very different depending on the initial fuel mass. This could be a problem because the initial available mass of propellant is difficult to predict before the mission due to unexpected additional maneuvers.

From an operational point of view, it is also interesting to see if the vehicle will collide with the surface in case of an engine re-ignition failure – a common failure in space missions. The trajectory without final braking burn is displayed in Fig.16. We can observe that the vehicle is on a collision course with Vesta and therefore will be destroyed if the final burn is not initiated, which represents an operational issue. A possible area for future investigation is to include in the optimization process the operational constraint of an abort orbit in case of an engine failure.

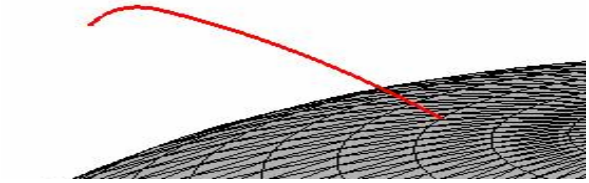

Fig. 16 Trajectory without final braking

IV.D.2 Optimal fuel strategy

The use of an optimal fuel strategy in decreasing the amount of propellant needed, as well as the sensitivity in initial mass, is discussed in this section. For clarity, only the trajectory and thrust magnitude are displayed in Fig. 17 and 18. As expected, this strategy is characterized by a longer descent coast and shorter braking phases.

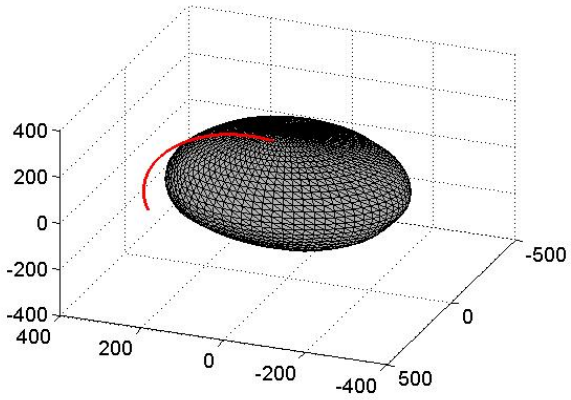

Fig. 17 Optimal fuel trajectory

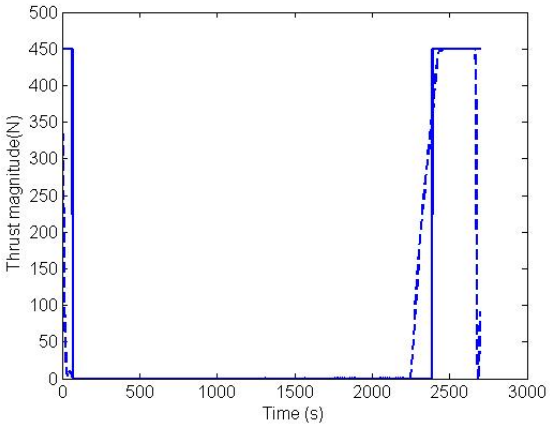

Fig. 18 Thrust magnitude

Table 3 summarizes the two main characteristics of each strategy.

	Opt. time strategy	Opt. fuel strategy
Time	15 min	45 min
Fuel	75 kg	50 kg

Table 3 Comparison of the two optimal strategies

The optimal fuel trajectory can save as much as 33 % of the propellant budget when compared to the optimal time trajectory. It is however 3 times longer.

In addition, we tested different initial fuel mass from 60kg to 100kg and very similar solutions were obtained contrary to the previous strategy.

V Landing simulation on Golevka

V.A Assumptions

Interplanetary trajectories to asteroids often require low-thrust propulsion systems since they are far more efficient than conventional chemical propulsion systems. Therefore, it would be interesting to study landing using the same electrical propulsion to avoid having two different kinds of engines. This is a feasible option at Golevka since it has a very low gravitational attraction. In this section, we will consider a xenon ion propulsion system with three Boeing 702 Thrusters characterized by 165 mN of thrust and 3800 seconds Isp.

Due to the high Isp, the fuel consumption will be very low, so we consider optimal time strategy only. Also to speed up the code, we suppose constant thrust at maximum magnitude – therefore no longer subject to optimization –, as well as constant mass. The equations of motion were modified in consequence.

Due to the irregular shape of Golevka and the perturbing solar radiation pressure, an orbiting spacecraft may exhibit chaotic motion and stability is therefore not guaranteed. Hence the traditional orbiter-type strategy is difficult to put in application. One alternative is body-fixed hovering, which fixes the spacecraft's position relative to the body by using thrusters to null the nominal accelerations on the spacecraft. Again, this approach is feasible for Golevka because of the relatively weak gravitational forces involved. At the desired hovering point $\mathbf{r}_0 = [x_0, y_0, z_0]^T$, thrust is defined as

$$\mathbf{T} = \left[\left.\frac{\partial U}{\partial x}\right|_0 - w^2 x_0, \left.\frac{\partial U}{\partial y}\right|_0 - w^2 y_0, \left.\frac{\partial U}{\partial z}\right|_0 \right]^T$$

V.B Hovering stability

As the parking orbit in the Vesta case, hovering is not stable everywhere. Sawai et al.[12] developed a set of criteria analytically that characterize the stability of a body-fixed hovering. These criteria were developed by linearizing the equations of motion about the hovering point :

$$3w^2 {v_{3z}}^2 + w^2 - (\alpha_1 + w^2) - (\alpha_2 + w^2) \geq 0$$
$$(\alpha_1 + w^2)(\alpha_2 + w^2) - w^2 {v_{1z}}^2 (\alpha_2 + w^2) - w^2 {v_{2z}}^2 (\alpha_1 + w^2) \geq 0$$
$$(\alpha_1 - \alpha_2 - w^2)^2 + 3w^4 {v_{3z}}^2 ({v_{3z}}^2 + 2) - 8w^2 {v_{3z}}^2 \left[(\alpha_1 + w^2) + (\alpha_2 + w^2)\right] > 0$$

where α_1, α_2, α_3 are the three eigenvalues of the Hessian matrix of the gravitational potential at $\mathbf{r}_0$ and v_1, v_2, v_3 are the corresponding eigenvectors.

The region of stability around Golevka defined by these three inequalities is displayed in Fig. 19 by the blue area. The hovering point is then chosen to be inside this region and in the direction of the normal to the landing site surface. A radius of 0.7km was selected since we found it was in the stability area at any latitude and longitude.

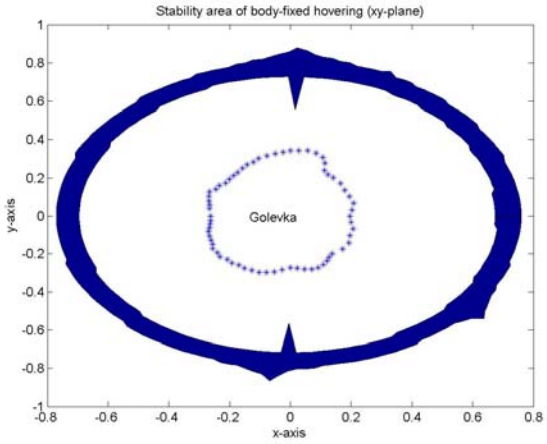

Fig. 19 Stability area of body-fixed hovering around Golevka (xy plane)

V.C Two-Point Boundary Value Problem formulation

The initial conditions are straightforward. All state variables are specified at the hovering point :

$$x(0) = x_0, y(0) = y_0, z(0) = z_0,$$
$$V_x(0) = 0, V_y(0) = 0, V_z(0) = 0 \qquad (14)$$

It follows that all co-state variables are free.

The final conditions are the same as those considered for Vesta.

The two-point boundary value problem is then stated as follows : the differential equations (1) and (4) (modified to suppose $T=T_{max}$ and $m=m_0$) are to be solved with the boundary conditions (3) and (14), while the optimal controls are described by equations (5)-(7).

V.D Simulation results

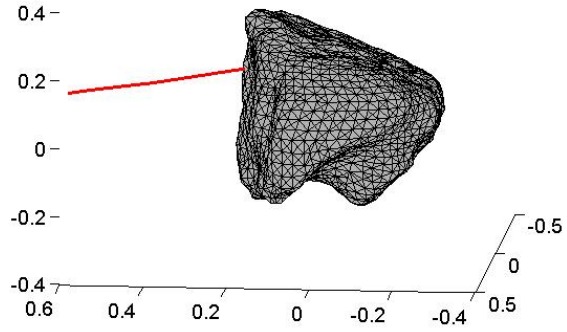

Fig. 18 Trajectory

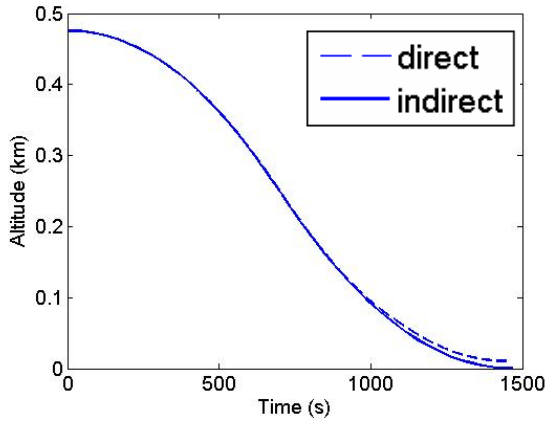

Fig. 19 Altitude

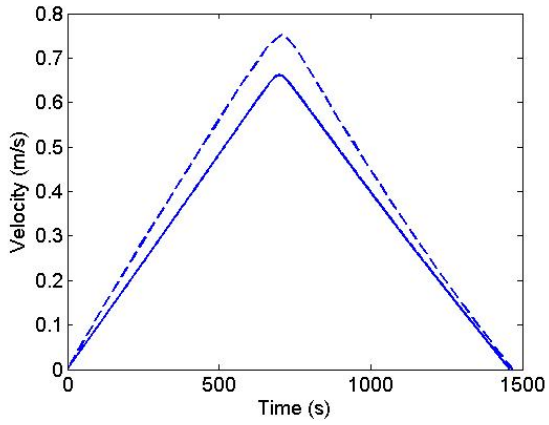

Fig. 20 Velocity magnitude

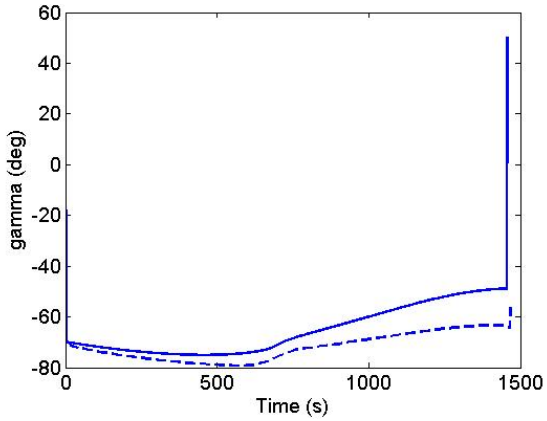

Fig. 21 Flight-Path angle

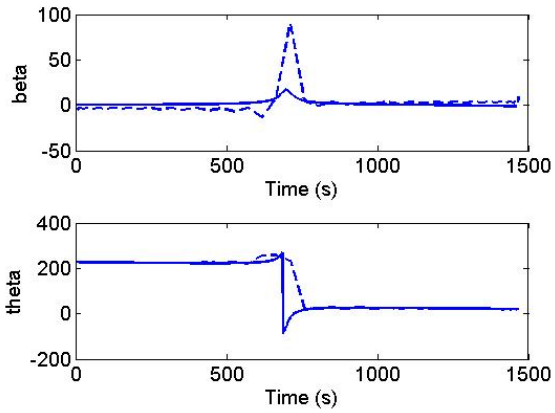

Fig. 22 Thrust directions

We can see that the trajectory is almost one-dimensional (straight line) with two distinct acceleration and deceleration phases.

Note in Fig. 19 that the final altitude value of the direct method is around 10m above the surface, which confirms that the direct solution is not exact.

VI Robustness

VI.A Parameter uncertainties

In the previous section, optimal trajectories have been obtained. However, it is also important to analyze their sensitivity with respect to parameter uncertainties and errors on controls and initial conditions. In fact, a non-robust optimal trajectory cannot be implemented for an operational standpoint. Here, the parameters affected by disturbances are :

- the body parameters : density, rotation rate, gravity field
- the initial orbit parameters
- the control states : thrust magnitude and directions

We will study two sets of covariances corresponding to different levels of precision in thrusters calibration and navigation. The uncertainties we used for the body parameters (density, rotation rate, and gravity field) are those found during NEAR Mission.[13] We assumed that the spacecraft visiting Vesta and Golevka can obtain the same level of certainty.

Covariance set	# 1	# 2
Density	0.05 %	0.05 %
Rotation rate	10^{-10} rad/s	10^{-10} rad/s
Gravity field	1 %	1 %
Initial Position	1 m	10 m
Initial Velocity	0.1 mm/s	5 mm/s
Thrust directions	0.1°	1°
Thrust magnitude	0.1 %	1 %

Table 4 One-sigma parameter uncertainties

A Monte-Carlo procedure with 5000 tries is applied in order to simulate these two sets of perturbed cases for descent trajectories on Vesta and Golevka.

VI.B Sensitivity simulations

VI.B.1 Vesta

Results for both optimal strategies are summarized in table 5. We considered only error in position for simplicity.

Run description		Range	
		Opt. time	Opt. fuel
#1	all	5.2 km	3.1 km
	Body parameters	2.5 km	3 km
	Controls	4 km	150 m
	Initial conditions	2 m	10 m
#2	all	8 km	4.5 km
	Body parameters	2.5 km	3 km
	Controls	6.5 km	1.7 km
	Initial conditions	13 m	80 m

Table 5 Contribution of parameter uncertainties to errors in position

A lot of interesting observations can be made from those results. First, errors due to parameter uncertainty in these descents are quite large, in the order of km. These errors are primarily due to body parameters and thrust errors. Because the necessary thrust is large to compensate the strong gravitational attraction of Vesta, any error in thrust magnitude or direction is causing a significant perturbing force leading to a high deviation from the nominal trajectory.

Also, we can see that the optimal-fuel strategy is surprisingly less sensitive to errors. This is unexpected because the longer the landing duration is, the more time it is subjected to these uncertainties. This can be explained by the effect of thrust errors explained above. Thruster uncertainties are the largest contributor to the miss distance in the optimal-time case because it applies full-thrust almost all along the trajectory. In the case of optimal-fuel strategy however, the ballistic phase is very long compared to braking phases, so thrust errors are less significant. This is another strong asset of the optimal-fuel strategy.

Moreover, regarding the sensitivity to errors in the initial conditions only, we can note that the magnitude of the error in final position is generally in the order of error in the initial position, which means that in this case the perturbed trajectory is similar to the nominal trajectory but starts at a slightly different location.

VI.B.2 Golevka

Range offsets and impact speeds are summarized in table 6.

	Cross range	Vertical range	Cross speed	Vertical speed
#1	3 m	2.5 m	3.7 mm/s	2.9 mm/s
#2	18.2 m	16.5 m	6.7 mm/s	10 mm/s

Table 6 One-sigma covariances of final position and velocity

Considering that this is applied in an open-loop manner, the magnitude of errors induced by covariance sets #1 and #2 are quite reasonable but it may be significant for some missions where high accuracy is required.

VI.C Real-time feedback control implementation

To improve the accuracy of landing, we need a fast numerical method to compute the future course of the optimal control variables during descent so that optimality is preserved even in the presence of those disturbances. Of course, the adjusted optimal control cannot be re-solved using the same method as in the previous sections because it cannot be practically realized in real-time. A simple approach is to locally linearize the perturbed dynamics about the undisturbed optimal trajectory :

$$\begin{cases} \delta\mathbf{x} = \mathbf{x}_p(t) - \mathbf{x}^*(t) \\ \delta\mathbf{u} = \mathbf{u}_p(t) - \mathbf{u}^*(t) \\ \delta\boldsymbol{\lambda} = \boldsymbol{\lambda}_p(t) - \boldsymbol{\lambda}^*(t) \end{cases}$$

The objective is to find the optimal $\delta\mathbf{u}^*$ so that the quadratic cost derived from the second variation of the problem is minimized. This method is called neighboring optimal control and the solution is the well-known feedback control.[14]

$$\delta\mathbf{u} = -H_{uu}^{-1}\mathbf{f}_u^T P\delta\mathbf{x} = K\delta\mathbf{x}$$

where P verifies the Ricatti equation

$$-\dot{P} = P\mathbf{f}_x + \mathbf{f}_x^T P - P\mathbf{f}_u H_{uu}^{-1}\mathbf{f}_u^T P$$

and $\mathbf{f}_x$, $\mathbf{f}_u$, H_{uu} are computed along the undisturbed optimal trajectory.

Since K does not depend on the disturbances and rely only on the unperturbed optimal trajectory data, it can be computed off-line and stored in an on-board computer.

This strategy is represented by the following block diagram.

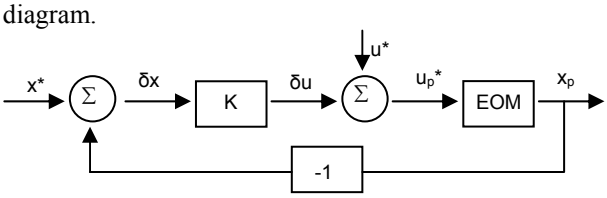

Fig. 23 Block diagram of the active controlled strategy

A case study for landing on Golevka with set #2 is presented in table 7. As expected, adding the controller improves the accuracy.

	Cross range	Vertical range
Without controller	18.2 m	16.5 m
With controller	2.5 m	3.5 m

Table 7 Effect of the controller on miss distance

However, we did not take into account the accuracy to which the spacecraft can estimate its position in the body-fixed frame (using optical navigation or altimetry). Large inaccuracy in those spacecraft-based measurements can cause severe error in final landing conditions. Future work will have to include those potential errors in the analysis.

VIIConclusion

We developed an efficient optimization algorithm to determine autonomous controlled landing trajectories on asteroids. It includes a precise and relatively fast model of the dynamical environment in the vicinity of asteroids. Then, two direct and indirect numerical methods have been combined to take advantage of both their merits and solve the optimal landing problem. Landing simulations on two very different asteroids Vesta and Golevka are shown as examples of the effectiveness of the code. A wide variety of options was investigated, including starting from a parking orbit or a hovering point, using liquid or electric propulsion, and two different optimal criteria – time or fuel. In particular, we have shown that the optimal-fuel strategy for Vesta is the most advantageous. It is efficient – lower amount of fuel necessary – and robust – lower dispersion and similar control law over a large range of initial conditions. More generally, any strategy involving long thrust maneuvers would probably be a bad choice for bodies as large as Vesta**.** Because a high thrust is necessary to compensate the gravitational attraction, any misalignment and magnitude error will perturb significantly the trajectory.

Future work could explore the effect of certain parameters that were held fixed in this study, like coordinates of the landing site, or characteristics and number of engines. Also, as figured out by Werner and Scheeres,[4] the algorithm to calculate the polyhedral gravity field can be readily coded using parallelization computations. Therefore, applying this idea in the future could make the code even faster and avoid the use of the approximate spherical harmonic gravity field.

This study could be easily extended to landing trajectories on cometary bodies or small moons orbiting giant planets. For the former class of bodies, a model for the outgassing of the comet nucleus and the related drag forces needs to be developed, whereas for the latter a simple tidal force can be added to the dynamical environment.

References

[1] "Solar System Exploration Roadmap", National Aeronautics and Space Administration, 2004.

[2] Dunham, D.W., Farquhar, R.W., McAdams, J.V., Holdridge, M., Nelson, R., Whittenburg, K., Antreasian, P., Chesley, S., Helfrich, C., Owen, W.M., Williams, B., Veverka, J., and Harch, A., "Implementation of the first asteroid landing", Icarus, Vol. 159, No. 2, 2002, pp. 433-438.

[3] http://www.psi.edu/pds/archive/asteroids.html

[4] Werner, R. A. and D. J. Scheeres, "Exterior gravitation of a polyhedron derived and compared with harmonic and mascon gravitation representations of asteroid 4769 Castalia", Celest. Mech. Dyn. Astr., 65, 313–344, 1997.

[5] Werner, R.A., "Spherical harmonic coefficients for the potential of a constant-density polyhedron", Comput. & Geosci. 23, 1071, 1997.

[6] Scheeres, D.J., "Satellite Dynamics about Small Bodies: Averaged Solar Radiation Pressure Effects," Journal of the Astronautical Sciences 47, 25–46, 1999.

[7] Kirk, D. E., "Optimal Control Theory – An Introduction", Prentice-Hall Networks Series, Prentice-Hall, Inc., Englewood Cliffs, NJ, 1970.

[8] Ross, I. M., "User's Manual for DIDO (Ver. PR.13): A MATLAB Application Package for Solving Optimal Control Problems," Technical Report 04-01.0, Naval Postgraduate School, Monterey, CA, February 2004.

[9] Oberle H.J., Grimm W., "BNDSCO – a program for the numerical solution of optimal control problems", Institute for Flight Systems Dynamics, DLR, Oberpfaffenhofen, Germany, Internal Report No. 515-89/22, 1989.

[10] Lara, M., and Scheeres, D. J., "Stability Bounds for Three-Dimensional Motion Close to Asteroids," Journal of the Astronautical Sciences, Vol. 50, No. 4, pp. 389–409, 2002.

[11] Wiesel, W., "Relative Satellite Motion About an Oblate Planet", Journal of Guidance, Control, and Dynamics, Vol. 25, No. 4, 2002.

[12] Sawai, S., Scheeres, D. J., and Broschart, S. B., "Control of Hovering Spacecraft Using Altimetry," Journal of Guidance, Control, and Dynamics, Vol. 25, No. 4, pp. 786–795, 2002.

[13] Miller, J.K., Konopliv, A.S., Antreasian, P.G., Bordi, J.J., Chesley, S., Helfrich, C.E., Owen, W.M.,Wang, T.C.,Williams, B.G., Yeomans, D.K., "Determination of Shape, Gravity, and Rotational State of Asteroid 433 Eros", Icarus, Vol. 155, No. 3-17, 2002.

[14] H. J. Pesch, "Numerical Computation of Neighboring Optimum Feedback Control Schemes in Real-Time," Appl. Math. Optim. 5, 231{252, 1979.